# Underactuated Control for Two-Wheeled Mobile Robot with an Arm Using Torque Constraint Conditions and Disturbance Observer

1st Jin Ito
*Graduate School of Integrated Design Engineering*
*Keio University*
Yokohama, Japan
ito@sum.sd.keio.ac.jp

2nd Toshiyuki Murakami
*Department of System Design Engineering*
*Keio University*
Yokohama, Japan
mura@sd.keio.ac.jp

2023 IEEE 32nd International Symposium on Industrial Electronics (ISIE) | 979-8-3503-9971-4/23/$31.00 ©2023 IEEE | DOI: 10.1109/ISIE51358.2023.10228153

***Abstract*—This paper presents an underactuated control system for a two-wheeled mobile robot (TWMR). TWMR is expected to use as an autonomous mobile robot (AMR) that works in human-collaborative spaces. TWMR has a smaller footprint and higher center of gravity (CoG), than typical AMRs. Furthermore, in this study, TWMR has an arm. Therefore, TWMR is superior in handling loads in human-presence spaces. However, TWMR is the underactuated system in the body's translational position and tilting angle. In addition, TWMR is affected by disturbances caused by loads. As a robust underactuated control system, the cascade PI/PD and synthesized pitch angle disturbance observer (SPADO) are considered. The cascade PI/PD results in significant translational position error and oscillatory responses. To cope with this problem, a proposed method minimizes both errors of the translational position and tilting angle within torque constraints. The proposed method utilizes the predictive functional control (PFC) for the underactuated control considering constraints. SPADO improves the accuracy of an internal model of PFC. The validity of the proposed method was confirmed compared with the cascade PI/PD through the simulation.**

***Index Terms*—underactuated control, two-wheeled mobile robot, torque constraints, predictive control, disturbance observer**

## I. Introduction

Autonomous mobile robots (AMRs) work together and assist humans in industry environments [1], [2]. AMR is expected to be used without modifying existing environments where humans work. However, typical AMRs have a larger footprint and a lower center of gravity (CoG) than humans because a typical AMR is a statically stable structure with three or more wheels. These features make AMR unsuitable for picking up loads and moving in facilities designed for humans. In this study, a two-wheeled mobile robot (TWMR) is proposed.

The proposed system, TWMR, is a double inverted pendulum robot. This system can perform various tasks by utilizing the second pendulum as an arm. Since TWMR has only two wheels, the footprint is small. Furthermore, TWMR has a high CoG because TWMR can stabilize itself by tilting the body. TWMR is better suited for working in human-collaborative spaces than general AMRs.

However, a pitch angle that is the tilting angle of the body is statically unstable. TWMR must move forward or backward to stabilize the pitch angle. Therefore, TWMR is the underactuated system in the translational position and pitch angle. Underactuated control methods for the two-wheeled mobile application can be applied to TWMR.

Pathak et al. [3] constructed independent control loops for the pitch angle and translational position respectively by the partial feedback linearization. Kim et al. [4] developed a robust nonlinear optimal control. These methods have the problem that the performances of controllers depend on modeling errors. Since TWMR handles objects by the arm, the model changes dynamically and modeling errors occur.

A cascade PI/PD controls both the translational position and pitch angle. PD controller controls the pitch angle in the minor loop and the PI controller controls the translational position indirectly in the major loop. However, a translational position error between the command and response is large because a pitch angle control frequency is faster. The translational position error generates a pitch angle command. Therefore, both responses oscillate.

The proposed method improves the robustness by using a synthesized pitch angle disturbance observer (SPADO) [5]. SPADO is a disturbance observer (DOB) [6] method designed for the two-wheeled mobile application. DOB can compensate for disturbances including modeling errors. The proposed method stabilizes TWMR by torque constraint conditions. The proposed method utilizes a predictive functional control (PFC) [7] to minimize both errors of the translational position and pitch angle within torque constraints. Since the proposed method compensates for modeling errors by SPADO, the internal model of PFC is accurate and robust. The proposed method is a novel underactuated controller based on PFC and DOB [8], [9]. Changes in the model due to loads are estimated from estimated torques by reaction torque observers (RTOBs) [10].

This paper is organized as follows: In section II, the model of TWMR is explained. In section III, the proposed controller is explained. In section IV, the simulation results are shown.

Authorized licensed use limited to: Keio University. Downloaded on October 03,2024 at 06:15:12 UTC from IEEE Xplore. Restrictions apply.

TABLE I: Parameters for TWMR

| Parameter | Explanation |
|---|---|
| $g$ | Gravitational acceleration |
| $\theta_{wr}$ | Right wheel angle |
| $\theta_{wl}$ | Left wheel angle |
| $d$ | Translational position of TWMR |
| $v$ | Translational velocity of TWMR |
| $\phi_v$ | Yaw angle of TWMR |
| $\theta_p$ | Pitch angle of body |
| $\theta_a$ | Arm angle |
| $L_t$ | Tread length of TWMR |
| $R_w$ | Radius of wheel |
| $L_p$ | Length between wheel axis and arm axis |
| $l_p$ | Length between wheel axis and CoG of the body |
| $l_a$ | Length between arm axis and CoG of arm |
| $m_b$ | Mass of body |
| $m_a$ | Mass of arm |
| $m_l$ | Mass of load |
| $l_l$ | Length between arm axis and position of load |
| $n_w$ | Gear ratio of wheel motor |
| $n_a$ | Gear ratio of arm motor |
| $\tau_r$ | Input torque of a right wheel motor |
| $\tau_l$ | Input torque of a left wheel motor |
| $\tau_a$ | Input torque of arm motor |

In section V, this paper is concluded.

## II. Modeling

In section II, the kinematics and dynamics of TWMR are described. The top and side views of the TWMR model are shown in Fig. 1. TWMR consists of the right wheel, left wheel, body, and arm. Each joint is equipped with a motor and gear. Parameters for TWMR are shown in Table I.

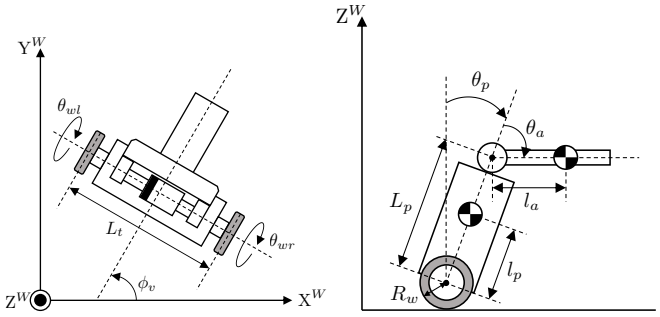


(a) Top view (b) Side view

Fig. 1: TWMR model

In this study, we assume that both wheels do not slip in either translational or lateral directions. A translational velocity and yaw rate of TWMR are described as (1), (2).

$$v = \frac{R_w}{2}\left(\dot{\theta}_{wr} + \dot{\theta}_{wl}\right) \tag{1}$$

$$\dot{\phi}_v = \frac{R_w}{L_t}\left(\dot{\theta}_{wr} - \dot{\theta}_{wl}\right) \tag{2}$$

A translational position of TWMR is defined as (3).

$$d(t) = \int_0^t v(\tau)d\tau \tag{3}$$

A joint space vector $\boldsymbol{q}$ is defined as (4).

$$\boldsymbol{q} = \begin{bmatrix} d & \phi_v & \theta_p & \theta_a \end{bmatrix}^\top \tag{4}$$

The dynamics of TWMR are described as (5).

$$\boldsymbol{M}(\boldsymbol{q})\ddot{\boldsymbol{q}} + \boldsymbol{C}(\boldsymbol{q}, \dot{\boldsymbol{q}}) + \boldsymbol{G}(\boldsymbol{q}) = \boldsymbol{E}\boldsymbol{\tau} \tag{5}$$

$\boldsymbol{M}$, $\boldsymbol{C}$, and $\boldsymbol{G}$ denote the inertia matrix, the torque caused by the centrifugal and Coriolis forces, and the torque caused by gravity. $\boldsymbol{E}$ is the coefficient matrix of input torques. $\boldsymbol{\tau}$ is the input torque vector. The matrices of (5) are described as (6) to (10).

$$\boldsymbol{M}(\boldsymbol{q}) = \begin{bmatrix} m_{11} & 0 & m_{13} & m_{14} \\ 0 & m_{22} & 0 & 0 \\ m_{31} & 0 & m_{33} & m_{34} \\ m_{41} & 0 & m_{43} & m_{44} \end{bmatrix} \tag{6}$$

$$\boldsymbol{C}(\boldsymbol{q}, \dot{\boldsymbol{q}}) = \begin{bmatrix} f_{c1} & \tau_{c2} & \tau_{c3} & \tau_{c4} \end{bmatrix}^\top \tag{7}$$

$$\boldsymbol{G}(\boldsymbol{q}) = \begin{bmatrix} 0 & 0 & \tau_{g3} & \tau_{g4} \end{bmatrix}^\top \tag{8}$$

$$\boldsymbol{E} = \begin{bmatrix} \frac{n_w}{R_w} & \frac{n_w}{R_w} & 0 \\ \frac{L_t n_w}{2R_w} & -\frac{L_t n_w}{2R_w} & 0 \\ -n_w & -n_w & 0 \\ 0 & 0 & n_a \end{bmatrix} \tag{9}$$

$$\boldsymbol{\tau} = \begin{bmatrix} \tau_r & \tau_l & \tau_a \end{bmatrix}^\top \tag{10}$$

## III. Control System Design

Section III describes the proposed control system. Fig. 2 shows the block diagram of the proposed system. The

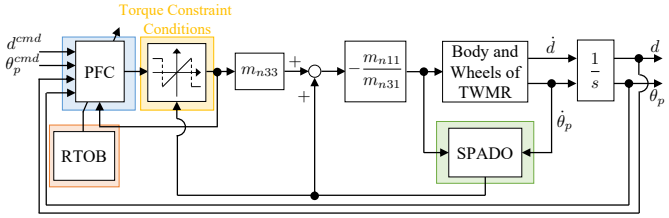


Fig. 2: Block diagram of the proposed system

proposed method consists of four components. The first section is SPADO. SPADO improves the robustness of the control system. The second section is PFC. PFC generates the input for both translational position and pitch angle control within torque constraints. The third section is torque constraint conditions. The conditions limit the PFC input to stabilize TWMR. The fourth section is RTOB. RTOB estimates the torque caused by gravity and external forces. The internal model of PFC is updated with estimated torques by RTOB.

### A. SPADO

Both translational position and pitch angle are controlled by a single input $f_d$. $f_d$ is described as (11).

$$f_d = \frac{n_w}{R_w}(\tau_r + \tau_l) \tag{11}$$

The inertias of TWMR after compensating disturbances caused by nonlinearities of dynamics, modeling errors, and external

Authorized licensed use limited to: Keio University. Downloaded on October 03,2024 at 06:15:12 UTC from IEEE Xplore. Restrictions apply.

forces are defined as nominal inertias. A nominal inertia matrix $\boldsymbol{M}_n$ is defined as (12).

$$\boldsymbol{M}_n = \begin{bmatrix} m_{n11} & 0 & 0 & 0 \\ 0 & m_{n22} & 0 & 0 \\ m_{n31} & 0 & m_{n33} & 0 \\ 0 & 0 & 0 & m_{n44} \end{bmatrix} \tag{12}$$

$\boldsymbol{M}_n$ is constant matrix. The translational position and pitch angle dynamics are shown in (13), (14).

$$m_{n11}\ddot{d} = f_d - f_d^{dis} \tag{13}$$

$$m_{n31}\ddot{d} + m_{n33}\ddot{\theta}_p = -\tau_p^{dis} \tag{14}$$

$f_d^{dis}$ is the disturbance force of translational position and $\tau_p^{dis}$ is the disturbance torque of pitch angle. SPADO estimates a synthesized disturbance torque $\tau_s^{dis}$. $\tau_s^{dis}$ is defined as (15). The relationship between $f_d$ and $\tau_s^{dis}$ is derived as (16).

$$\tau_s^{dis} = \tau_p^{dis} - \frac{m_{n31}}{m_{n11}} f_d^{dis} \tag{15}$$

$$m_{n33}\ddot{\theta}_p + \tau_s^{dis} = -\frac{m_{n31}}{m_{n11}} f_d \tag{16}$$

An estimated synthesized disturbance torque $\hat{\tau}_s^{dis}$ is described as (17) by using a low-pass filter (LPF). $g_{sp}$ is the cut-off angular frequency of LPF.

$$\hat{\tau}_s^{dis} = \frac{g_{sp}}{s + g_{sp}} \left( -\frac{m_{n31}}{m_{n11}} f_d + g_{sp} m_{n33} \dot{\theta}_p \right) - g_{sp} m_{n33} \dot{\theta}_p \tag{17}$$

SPADO compensates $\tau_s^{dis}$ in the bandwidth of the cut-off frequency. Fig. 3 shows the block diagram of SPADO. SPADO

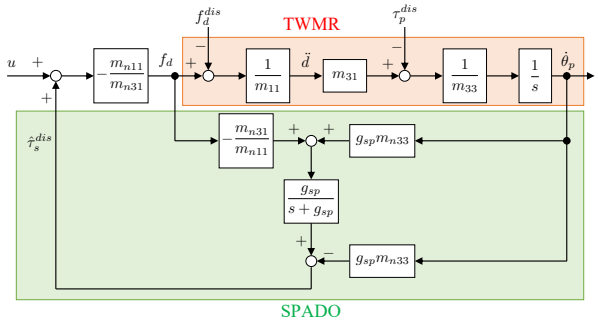


Fig. 3: Block diagram of SPADO

compensates for the pitch angle disturbance $\tau_p^{dis}$ by using translational acceleration $\ddot{d}$ as a pseudo-input.

## B. PFC

PFC is one type of model predictive control (MPC) strategy. PFC generates the input without real-time optimization, considering input constraints. Therefore, PFC has a smaller computational load and higher control frequency than general MPC. In the proposed method, PFC controls the translational position and pitch angle within torque constraints.

*a) Internal Model:* An internal model of PFC consists of TWMR and SPADO. Since SPADO uses $\ddot{d}$ as a pseudo-input, the dynamics of $d$ is affected by $\hat{\tau}_p^{dis}$. Therefore, the internal model is robust, but cannot eliminate $\hat{\tau}_p^{dis}$. $\hat{\tau}_p^{dis}$ can be approximated as torque by gravity and external forces. The internal model of PFC, the discrete-time state space model is described as (18), (19).

$$\boldsymbol{x}_M[k+1] = \boldsymbol{A}_M \boldsymbol{x}_M[k] + \boldsymbol{B}_M u_{pfc}[k] + \boldsymbol{E}_M \tag{18}$$

$$\boldsymbol{y}_M[k] = \boldsymbol{C}_M \boldsymbol{x}_M[k] \tag{19}$$

The matrices of the internal model are described as (20) to (24).

$$\boldsymbol{x}_M = \begin{bmatrix} d[k] & \theta_p[k] & \dot{d}[k] & \dot{\theta}_p[k] \end{bmatrix}^\top \tag{20}$$

$$\boldsymbol{A}_M = \begin{bmatrix} 1 & 0 & T_s & 0 \\ 0 & 1 & 0 & T_s \\ 0 & \frac{T_s a_1}{R_w m_{n11} + m_{n31}} & 1 & 0 \\ 0 & 0 & 0 & 1 \end{bmatrix} \tag{21}$$

$$\boldsymbol{B}_M = \begin{bmatrix} 0 & 0 & -\frac{T_s m_{n33}}{R_w m_{n11} + m_{n31}} & T_s \end{bmatrix}^\top \tag{22}$$

$$\boldsymbol{C}_M = \begin{bmatrix} 1 & 0 & 0 & 0 \\ 0 & 1 & 0 & 0 \end{bmatrix} \tag{23}$$

$$\boldsymbol{E}_M = \begin{bmatrix} 0 & 0 & \frac{T_s b_1}{R_w m_{n11} + m_{n31}} & 0 \end{bmatrix}^\top \tag{24}$$

$$a_1 = \{ m_b l_p + (m_a + m_l) L_p \} g \tag{25}$$

$$b_1 = -m_a l_a g \sin(\theta_p + \theta_a) - m_l l_l g \sin(\theta_p + \theta_a) \tag{26}$$

$T_s$ is a sampling period of PFC.

*b) PFC Controller Design:* The control input of PFC is the weighted sum of polynomial basis functions. $n_B$ is the maximum degree of basis functions and the control input is described as (27).

$$u_{pfc}[k+i] = \sum_{l=0}^{n_B - 1} \mu_l[k] i^l \tag{27}$$

$\mu_l[k]$ is the unknown weighted coefficient, which is the optimization variable in PFC. The reference trajectory $\boldsymbol{y}_R[k+i]$ in a prediction horizon is defined as (28).

$$\boldsymbol{y}_R = \boldsymbol{s}[k+i] - \alpha^i (\boldsymbol{s}[k] - \boldsymbol{y}_P[k]) \tag{28}$$

$\boldsymbol{s}$ is the output command and $\boldsymbol{y}_P$ is the observed output. $\alpha$ is a damping factor and is defined as (29).

$$\alpha = e^{-\frac{3T_s}{T_{CLRT}}} \tag{29}$$

$T_{CLRT}$ is the Closed-Loop Response Time, which determines the response speed. PFC optimizes errors between output predictions and the reference trajectory at only coincidence points, not all sample points in the prediction horizon. The coincidence points $h_j$ are defined as (30). $n_h$ is the number of coincidence points.

$$h_j = \frac{T_{CLRT}}{T_s (n_h - j + 1)} \quad (j = 1, \cdots, n_h) \tag{30}$$

Authorized licensed use limited to: Keio University. Downloaded on October 03,2024 at 06:15:12 UTC from IEEE Xplore. Restrictions apply.

The PFC's evaluation function $J[k]$ is defined as (31).

$$J[k] = \sum_{j=1}^{n_h} \|\hat{\boldsymbol{y}}_P[k+h_j] - \boldsymbol{y}_R[k+h_j]\|^2 \tag{31}$$

$\hat{\boldsymbol{y}}_P$ is the output prediction and is derived from the internal model. In this study, $n_B$ and $n_h$ are set to 3. Therefore, an optimization parameter $\boldsymbol{\mu}$, which minimizes $J[k]$ is described as (32).

$$\begin{aligned}\boldsymbol{\mu}[k] &= \begin{bmatrix}\mu_0[k] & \mu_1[k] & \mu_2[k]\end{bmatrix}^\top \\ &= \boldsymbol{G}_F^+ \begin{bmatrix} (\boldsymbol{s}[k] - \boldsymbol{y}_P[k])\left(1-\alpha^{h_1}\right) + \boldsymbol{C}_M\left(\boldsymbol{I} - \boldsymbol{A}_M^{h_1}\right)\boldsymbol{x}_M[k] \\ (\boldsymbol{s}[k] - \boldsymbol{y}_P[k])\left(1-\alpha^{h_2}\right) + \boldsymbol{C}_M\left(\boldsymbol{I} - \boldsymbol{A}_M^{h_2}\right)\boldsymbol{x}_M[k] \\ (\boldsymbol{s}[k] - \boldsymbol{y}_P[k])\left(1-\alpha^{h_3}\right) + \boldsymbol{C}_M\left(\boldsymbol{I} - \boldsymbol{A}_M^{h_3}\right)\boldsymbol{x}_M[k] \end{bmatrix}\end{aligned} \tag{32}$$

$$\boldsymbol{G}_F = \begin{bmatrix} \boldsymbol{G}_0[h_1] & \boldsymbol{G}_1[h_1] & \boldsymbol{G}_2[h_1] \\ \boldsymbol{G}_0[h_2] & \boldsymbol{G}_1[h_2] & \boldsymbol{G}_2[h_2] \\ \boldsymbol{G}_0[h_3] & \boldsymbol{G}_1[h_3] & \boldsymbol{G}_2[h_3] \end{bmatrix} \tag{33}$$

$$\boldsymbol{G}_p[i] = \sum_{q=1}^{i} \boldsymbol{C}_M \boldsymbol{A}_M^{q-1} \boldsymbol{B}_M \left((i-q)\,T_s\right)^p \quad (p = 0,1,2) \tag{34}$$

$$\boldsymbol{G}_F^+ = \boldsymbol{G}_F^\top \left(\boldsymbol{G}_F \boldsymbol{G}_F^\top\right)^{-1} \tag{35}$$

$\boldsymbol{G}_F$ is not a square matrix because the internal model is a single-input multi-output (SIMO) system. Therefore, the proposed method utilizes $\boldsymbol{G}_F^+$, the pseudo-inverse matrix of $\boldsymbol{G}_F$. The actual PFC control input is the first element of $\boldsymbol{\mu}$. The input is described as (36).

$$u_{pfc}[k] = \mu_0[k] \tag{36}$$

### C. Torque Constraint Conditions

Fig. 4 shows the block diagram of the PFC controller and torque constraint conditions. $\tilde{u}_{pfc}$ is a limited value of the

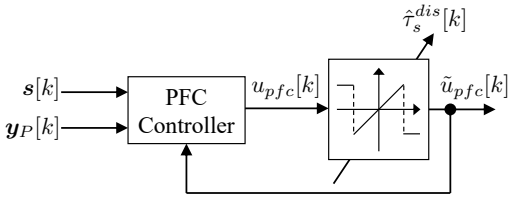


Fig. 4: Block diagram of the torque constraint conditions

PFC input. The proposed method considers torque constraints by feedbacking the limited input $\tilde{u}_{pfc}$ directly to the PFC controller. The limited value $f_d^{limit}$ is defined as (37) by using the limit value of the wheel motor torque $\tau^{limit}$.

$$f_d^{limit} = \frac{2n_w}{R_w}\tau^{limit} \tag{37}$$

The input $f_d$ consists of the PFC input and SPADO torque. A minimum and maximum value of $u_{pfc}$ are defined as (38), (39).

$$u_{min}[k] = \frac{1}{m_{n33}}\left(\frac{m_{n31}}{m_{n11}} f_d^{limit} - \hat{\tau}_s^{dis}[k]\right) \tag{38}$$

$$u_{max}[k] = \frac{1}{m_{n33}}\left(-\frac{m_{n31}}{m_{n11}} f_d^{limit} - \hat{\tau}_s^{dis}[k]\right) \tag{39}$$

The limited input $\tilde{u}_{pfc}$ is determined from torque constraint conditions (40).

$$\tilde{u}_{pfc}[k] = \begin{cases} u_{max}[k] & (u_{pfc} < u_{min}) \\ u_{pfc}[k] & (u_{min} \le u_{pfc} \le u_{max}) \\ u_{min}[k] & (u_{max} < u_{pfc}) \end{cases} \tag{40}$$

In the constraint conditions, the limited input $\tilde{u}_{pfc}$ is set to $u_{max}$ when $u_{pfc}$ is less than $u_{min}$ and set to $u_{min}$ when $u_{pfc}$ is greater than $u_{max}$ to stabilize TWMR.

### D. RTOB

RTOBs are introduced to estimate the torques of the body and arm caused by gravity and external forces. The estimated torques are described as (41), (42).

$$\begin{aligned}\hat{\tau}_p^{rtob} =& \frac{g_{rp}}{s+g_{rp}}\left(-R_w f_d + g_{rp}\boldsymbol{m}_3\dot{\boldsymbol{q}} - \tau_{c3} - \tau_p^{fric}\right) \\ &- g_{rp}\boldsymbol{m}_3\dot{\boldsymbol{q}}\end{aligned} \tag{41}$$

$$\begin{aligned}\hat{\tau}_a^{rtob} =& \frac{g_{ra}}{s+g_{ra}}\left(n_a\tau_a + g_{ra}\boldsymbol{m}_4\dot{\boldsymbol{q}} - \tau_{c4} - \tau_a^{fric}\right) \\ &- g_{ra}\boldsymbol{m}_4\dot{\boldsymbol{q}}\end{aligned} \tag{42}$$

$g_{rp},\ g_{ra}$ are the cut-off angular frequencies. $\tau_p^{fric},\ \tau_a^{fric}$ are friction torques. $\boldsymbol{m}_3,\ \boldsymbol{m}_4$ are the third and fourth-row vectors of the inertia matrix $\boldsymbol{M}(\boldsymbol{q})$. $\hat{\tau}_p^{rtob},\ \hat{\tau}_a^{rtob}$ can be used to estimate the parameters $a_1$ and $b_1$ as (43), (44).

$$a_1 = -\frac{\hat{\tau}_p^{rtob} - \hat{\tau}_a^{rtob}}{\sin\theta_p} \tag{43}$$

$$b_1 = \hat{\tau}_a^{rtob} \tag{44}$$

The internal model of PFC is updated by utilizing (43), (44).

### E. Nominal Inertia Tuning

The nominal inertia matrix is set to the value when $\theta_p$ is 0 degrees and $\theta_a$ is 90 degrees. $B_3,\ B_4$ are the third and fourth elements of the input vector $\boldsymbol{B}_M$ and described as (45), (46).

$$B_3 = -\frac{T_s m_{n33}}{R_w m_{n11} + m_{n31}} \tag{45}$$

$$B_4 = T_s \tag{46}$$

$B_3,\ B_4$ are input coefficients of $\dot{d}[k],\ \dot{\theta}_p[k]$ for the single input $f_d$. $B_3,\ B_4$ have effects on the dynamics of the TWMR. In this study, the values of $B_3$ and $B_4$ are adjusted to stabilize the TWMR by changing the nominal inertia matrix.

## IV. Simulation

In section IV, the simulation results are shown. The simulation compared the proposed method with the conventional method in the presence of disturbance by the load.

Authorized licensed use limited to: Keio University. Downloaded on October 03,2024 at 06:15:12 UTC from IEEE Xplore. Restrictions apply.

### A. Controller Setup

Fig. 5 shows the block diagram of the whole system. The DOB+PD control system is constructed for the arm and

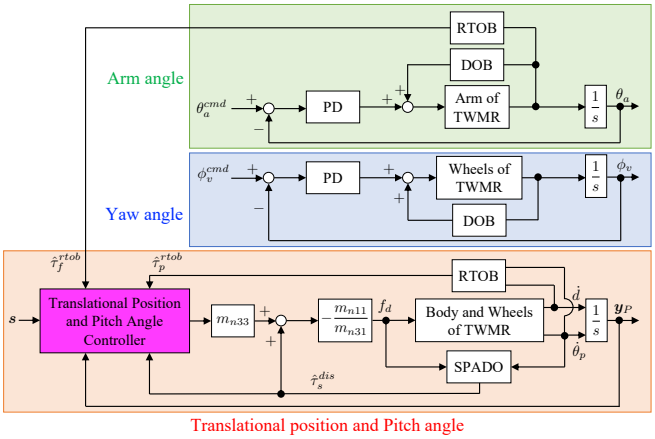


Fig. 5: Block diagram of the whole system

yaw angles, respectively. The arm angle is controlled to be horizontal to the ground. The simulation does not consider the turning of the TWMR. $\theta_a^{cmd}$, $\phi_v^{cmd}$ is defined as (47), (48).

$$\theta_a^{cmd} = \pi/2 - \theta_p \tag{47}$$

$$\phi_v^{cmd} = 0 \tag{48}$$

The pitch angle command $\theta_p^{cmd}$ is described as (49) from the dynamics of the translational position $d$ in (18).

$$\begin{aligned}\theta_p^{cmd} =& \frac{R_w m_{n11} + m_{n31}}{a_1}\ddot{d}^{cmd} + \frac{-b_1}{a_1} \\ =& \theta_p^{acc} + \theta_p^{rtob}\end{aligned} \tag{49}$$

$\theta_p^{cmd}$ is the angle at which the pitch angle is stable, including the effects of loads, when TWMR accelerates at $\ddot{d}^{cmd}$. $\theta_p^{cmd}$ consists of $\theta_p^{acc}$ and $\theta_p^{rtob}$. $\theta_p^{acc}$ is determined by the acceleration command $\ddot{d}^{cmd}$. $\theta_p^{rtob}$ is derived from $a_1$, $b_1$, which is estimated parameters by RTOB. $\theta_p^{rtob}$ is added to cancel the disturbance. In the proposed method, $\theta_p^{cmd}$ is discretized by a sampler with sampling period $T_s$.

The conventional method is a cascade PI/PD. Fig. 6 shows the cascade PI/PD block diagram. In the cascade PI/PD, the

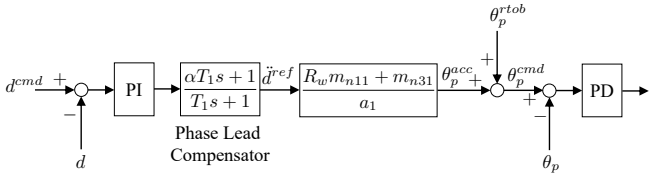


Fig. 6: Block diagram of the cascade PI/PD

PI controller controls the translational position. PD controller controls the pitch angle. The phase lead compensator stabilizes the major loop of the translational position.

TABLE II: Parameters used in the simulation

| Parameter | Value | Explanation |
|---|---|---|
| $g_{sp}$ (rad/s) | $2\pi \times 4$ | Cut-off angular frequency of SPADO |
| $g_{rd}$ (rad/s) | $2\pi \times 4$ | Cut-off angular frequency of DOB for $\phi_v$ |
| $g_{ad}$ (rad/s) | $2\pi \times 5$ | Cut-off angular frequency of DOB for $\theta_a$ |
| $g_{rp}$ (rad/s) | $2\pi \times 15$ | Cut-off angular frequency of RTOB for $\theta_p$ |
| $g_{ra}$ (rad/s) | $2\pi \times 15$ | Cut-off angular frequency of RTOB for $\theta_a$ |
| $\tau^{limit}$ (Nm) | 1.25 | Limit value of a wheel motor torque |
| $K_{pp}$ (/s$^2$) | 100 | P-gain for $\theta_p$ |
| $K_{dp}$ (/s) | 20 | D-gain for $\theta_p$ |
| $K_{pt}$ (/s$^2$) | 0.50 | P-gain for $d$ |
| $K_{it}$ (−) | 0.065 | I-gain for $d$ |
| $K_{pf}$ (/s$^2$) | 100 | P-gain for $\theta_a$ |
| $K_{df}$ (/s) | 20 | D-gain for $\theta_a$ |
| $K_{pr}$ (/s$^2$) | 100 | P-gain for $\phi_v$ |
| $K_{dr}$ (/s) | 20 | D-gain for $\phi_v$ |
| $\alpha$ (−) | 2.04 | Ratio of phase lead compensator |
| $T_1$ (s/rad) | 1.75 | Parameter for phase lead compensator |
| $T_s$ (s) | $1.0 \times 10^{-3}$ | Sampling period |
| $T_{CLRT}$ (s) | 0.20 | Closed loop response time |

Unlike the proposed method, the cascade PI/PD derives $\theta_p^{acc}$ from $\ddot{d}^{ref}$ generated by the PI controller. Therefore, the translational position error affects $\theta_p^{cmd}$ in the cascade PI/PD. As a result, both the pitch angle response and the translational position response oscillate.

The parameters used in the simulation are shown in Table II.

### B. Simulation Results

The TWMR was loaded with a 3 kg load and given a position command $d^{cmd}$. $d^{cmd}$ is derived from a trapezoidal velocity command and described as (50).

$$d^{cmd} = \begin{cases} 0.75t^2 & (0 \le t \le 5) \\ 7.5t - 18.75 & (5 < t \le 10) \\ -0.75t^2 + 22.5t - 93.75 & (10 < t \le 15) \\ 75 & (15 < t \le 20) \end{cases} \tag{50}$$

$d^{cmd}$ is a command value that causes TWMR to accelerate, move at a constant velocity, decelerate, and stop at 5-second intervals. The translational position and pitch angle simulation results are shown in Fig. 7 and Fig. 8, respectively.

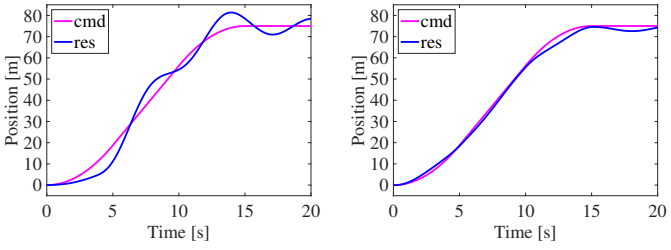


(a) Conventional method (b) Proposed method

Fig. 7: Translational position

In the conventional method, the translational position response oscillated, while in the proposed method, the response did not oscillate and followed the command. The tracking performance of the proposed method was improved.

Authorized licensed use limited to: Keio University. Downloaded on October 03,2024 at 06:15:12 UTC from IEEE Xplore. Restrictions apply.

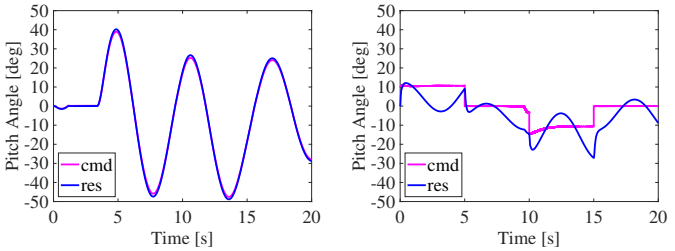


(a) Conventional method (b) Proposed method

Fig. 8: Pitch angle

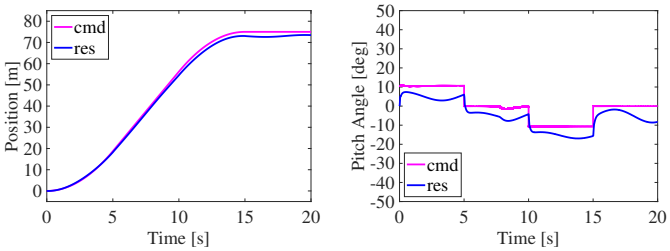


(a) Translational position (b) Pitch angle

Fig. 10: Alternative conditions

The tracking performance of the pitch angle control appeared to be better with the conventional method. However, the conventional method generated a pitch angle command $\theta_p^{cmd}$ from $\ddot{d}^{ref}$, resulting in large oscillations in the command itself. The amplitude of the pitch angle oscillation was $-50$ to $40$ degrees, which might cause TWMR to fall over. In the proposed method, however, the pitch angle command did not oscillate and the pitch angle was stabilized.

Fig. 9 shows the control input $f_d$. In the proposed method,

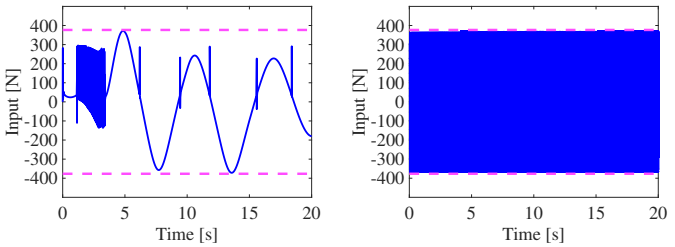


(a) Conventional method (b) Proposed method

Fig. 9: Control input $f_d$

the input was limited in the range of the constraint. The input of the proposed method oscillated at a higher frequency than the conventional method. It is thought that the control performance was enhanced because the input changed quickly to increases in errors.

As a result, it is confirmed that the proposed method improved both the translational position and pitch angle control performance within torque constraints compared to the conventional method.

### C. Alternative torque constraint conditions

Alternative torque constraint conditions (51) to (40) were applied to the proposed method.

$$\tilde{u}_{pfc}[k] = \begin{cases} u_{max}[k] & (u_{pfc} \leq u_{max}) \\ u_{min}[k] & (u_{max} < u_{pfc}) \end{cases} \tag{51}$$

Simulation results using (51) are shown in Fig. 10. The alternative conditions (51) suppress response oscillations relative to the conditions (40). The PFC input $u_{pfc}$ is used only to determine if the constraints are exceeded. Using the maximum value at each step is considered to suppress response oscillations more than the PFC input, which minimizes the errors.

## V. Conclusion

This study proposed a robust underactuated control system utilizing PFC and SPADO. The proposed method controls both the translational position and the pitch angle of TWMR with only a single input within torque constraints. The simulation results show that the proposed method is effective in the presence of disturbance. Torque constraint conditions suitable for TWMR control will be proposed in future work.

## References

[1] M. A. K. Niloy et al., "Critical Design and Control Issues of Indoor Autonomous Mobile Robots: A Review," in IEEE Access, vol. 9, pp. 35338-35370, 2021.

[2] R. S. Pol and M. Murugan, "A review on indoor human aware autonomous mobile robot navigation through a dynamic environment survey of different path planning algorithm and methods," 2015 International Conference on Industrial Instrumentation and Control (ICIC), Pune, India, 2015, pp. 1339-1344.

[3] K. Pathak, J. Franch and S. K. Agrawal, "Velocity and position control of a wheeled inverted pendulum by partial feedback linearization," in IEEE Transactions on Robotics, vol. 21, no. 3, pp. 505-513, June 2005.

[4] S. Kim and S. Kwon, "Nonlinear Optimal Control Design for Underactuated Two-Wheeled Inverted Pendulum Mobile Platform," in IEEE/ASME Transactions on Mechatronics, vol. 22, no. 6, pp. 2803-2808, Dec. 2017.

[5] A. Dinale, K. Hirata and T. Murakami, "Analytical design of a robust motion controller for a two-wheeled wheelchair system," 2013 16th International Conference on Advanced Robotics (ICAR), Montevideo, Uruguay, 2013, pp. 1-6.

[6] K. Ohnishi, "Robust Motion Control by Disturbance Observer," Journal of the Robotics Society of Japan, vol. 11, Issue 4, pp. 486-493, 1993.

[7] J. Richalet, S. Abu El Ata-Doss, C. Arber, H.B. Kuntze, A. Jacubasch, and W. Schill, "Predictive Functional Control - Application to Fast and Accurate Robots," in IFAC Proceedings Volumes, Vol. 20, No. 5, pp. 251-258, 1987.

[8] H. Liu and S. Li, "Speed Control for PMSM Servo System Using Predictive Functional Control and Extended State Observer," in IEEE Transactions on Industrial Electronics, Vol. 59, No. 2, pp. 1171-1183, Feb, 2012.

[9] T. Ohhira, K. Yokota, S. Tatsumi and T. Murakami, "A Robust Hybrid Position/Force Control Considering Motor Torque Saturation," in IEEE Access, vol. 9, pp. 34515-34528, 2021.

[10] T. Murakami, F. Yu and K. Ohnishi, "Torque sensorless control in multidegree-of-freedom manipulator," in IEEE Transactions on Industrial Electronics, vol. 40, no. 2, pp. 259-265, April 1993.

Authorized licensed use limited to: Keio University. Downloaded on October 03,2024 at 06:15:12 UTC from IEEE Xplore. Restrictions apply.